Renewable and Sustainable Energy Reviews 15 (2011) 4053–4066

Contents lists available at ScienceDirect

Renewable and Sustainable Energy Reviews

journal homepage: www.elsevier.com/locate/rser

Performance modeling and investigation of fixed, single and dual-axis tracking photovoltaic panel in Monastir city, Tunisia

Taher Maatallah, Souheil El Alimi*, Sassi Ben Nassrallah

Energy and Thermal Systems Laboratory, National Engineering School of Monastir, University of Monastir, Avenue Ibn El Jazzar 5019, Tunisia

ARTICLE INFO

Article history:
Received 20 December 2010
Received in revised form 9 May 2011
Accepted 5 July 2011
Available online 21 August 2011

Keywords:
Solar radiation basic photovoltaic modeling
PV generation
Optimal angles
Tracking systems
Gain

ABSTRACT

Presented in this paper was an overview on research works on solar radiation basics and photovoltaic generation. Also, a complete PV modeling and investigation on the effect of using multi-axes sun-tracking systems on the electrical generation was carried out to evaluate its performance using the case study of the Monastir city, Tunisia. The effects of azimuth and tilt angles on the output power of a photovoltaic module were investigated. The instantaneous increments of the output power generated by a photovoltaic module mounted on a single and dual-axis tracking system relative to a traditional fixed panel were estimated. The results show that the yearly optimal tilt angle of a fixed panel faced due to the south is close to 0.9 times Monastir latitude. The gain made by the module mounted on a single-axis tracking panel relative to a traditional fixed panel was analyzed. The monthly increments of the gain are more noticeable for two critical periods which correspond to those surrounding the summer and the winter solstice dates. It reaches the value of 10.34% and 15% in the summer and winter solstice periods, respectively. However, the yearly gain relative to a fixed panel installed with the yearly optimal tilt angle is 5.76%. In some applications, covering loads at early morning or late afternoon hours and in order to more optimize the solar systems exploitation suggest the adjustment of the PV panel orientation to azimuth angles different from the south direction by using a dual-axis tracking installation. The gain made by this recommendation relative to a traditional fixed panel is evaluated. This gain reaches 30% and 44% respectively in the winter and summer solstice days.

Contents

* Corresponding author. Tel.: +216 98452098; fax: +216 73907975.
E-mail address: souheil.elalimi@gmail.com (S. El Alimi).

1364-0321/$ – see front matter © 2011 Elsevier Ltd. All rights reserved.
doi:10.1016/j.rser.2011.07.037

1. Introduction

Renewable energy resources have enormous potential and can satisfy the present world energy demand. They can enhance diversity in energy supply markets, secure long-term sustainable energy supply, and reduce local and global atmospheric emissions [1]. One of the important renewable energy is the solar energy which can be captured anywhere and can be directly converted into electric power through PV panels [2] which allow the production of electricity using photovoltaic cells that convert solar irradiation into useable electricity and, as a result, have become one of the most reliable sources of low pollutant energy. Besides, PV energy production represents an environmentally advantageous and sustainable method of maintaining an energy intensive standard of living [3–5].

The use of photovoltaic panels was originally planned as a type of technology to be used for external space applications [6–11]. The PV applications have been harnessed in various areas such as water pumping, rural electrification, remote meteorological stations, maritime and railway crossing, production of hydrogen, grid connection systems, refrigeration, low power rural industrial applications, etc. [12–26].

On the other hand, recent technological advancements have stimulated the development and the use of PV panels in the commercial market for its use in building appliances. Regardless of its requisite high primary costs, PV systems have been adopted in many countries as an efficient means of producing energy in rural and urban areas that show a higher output in rural areas [27]. Thereby, the worldwide annual development rate in PV industry has averaged more than 30% in the last decade [28,29].

A PV module is composed of several solar cells. The output power of a PV module is mainly based on two factors, i.e. cell temperature and solar radiation incident on it [30]. The intensity of incident solar radiation on a panel is affected by the installation azimuth and tilt angle, as both angles influence the incident angle of sunlight on it. The optimal angles vary with conditions such as the geographic latitude, climate, atmospheric composition, utilization period and so forth [31,32]. It is known that the optimum value of yearly maximum output energy can be obtained from PV modules oriented facing south and the optimum tilt angle is equal to the local latitude [33,34]. However the optimal tilt angle varies significantly with the geographic latitude, climate condition, utilization period of time, etc. [35,36].

It is widely acknowledged that Southern orientation for PV panels in the Northern Hemisphere is optimal and because that result indicate that an average of 98.6% a system's performance with the optimal angle can be obtained using the latitude angle for the tilted panel [37].

Many empirical correlations are available in literature for estimating the optimum tilt angle under various operational conditions. It is found that the optimum value of yearly maximum output energy can be obtained from PV modules oriented facing south with a tilt angle in the range of 20–30° [38]. Duffie and Beckman [33] suggested the use of (latitude + 15°) ±15° where the plus and minus signs correspond to the use in winter and summer, respectively. Chow and Chan [39] analyzed the irradiation data measured in a coastal region of South China and found that, over a year, solar collectors should be placed with a tilt angle of 2.8° greater than the latitude with the azimuth facing south-west. Shariah et al. [40] showed that the yearly optimum inclination angle for solar collectors in Jordan is less than the latitude by about 5–8°.

Gunerhan and Hepbasli [41] found that the optimal angles for solar collectors in Izmir, Turkey were in good agreement with those calculated by the expressions proposed by Nijegorodov et al. [42] which consist of a 12 expressions set for determining the monthly optimal tilt angle for latitudes between 60° north and 60° south. However, Yakup and Malik [43] found that the optimum tilt angles in Brunei Darussalam were almost less than the ones calculated by [42], due to the change in radiation patterns from location to location.

The performance analysis mentioned above are not yet sufficient, because they use usually monthly mean values of daily solar irradiation on inclined surfaces. However, in many cases, these values are not sufficient, because they do not allow a precise idea of the different energy phenomena, which take place in the heart of the production system (inertia phenomenon, shadowing masks, etc.). So, it is very important to study the instantaneous performance of PV arrays at different tilt angles and azimuths.

In this paper, an evaluation study and an overview on research works of all over the solar basics and photovoltaic generation are presented. The mentioned models can be considered as the representative of worldwide average. Its details can be found therein. Furthermore, many factors that affect the instantaneous PV production are analyzed for specific days in different situations using the case study of Monastir city. Also, the amount of extra output power generated by a single-axis tracked panel relative to fixed panel, installed with the yearly optimal tilt angle which is computed before, are estimated in this paper.

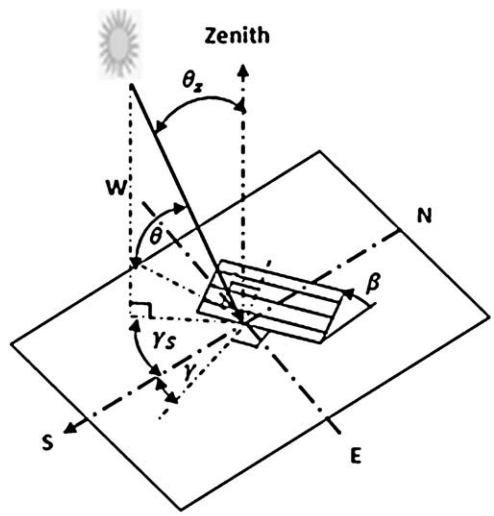


Fig. 1. Zenith angle, slope, surface azimuth angle and solar azimuth angle for a tilted surface.

Finally, the gains made by a dual-axis tracked panel are evaluated.

2. Solar radiation basic: an overview

The sun, with a diameter of 1.39×10^9 m, emit a total energy output of 3.8×10^{20} MW, however only a tiny fraction of 1.7×10^{14} kW is captured by the earth after traveling a mean distance of 1.495×10^{11} m [44]. The eccentricity of the earth's orbit is such the distance between the sun and the earth varies by 1.7% [33]. Further sun–earth geometric relationships will be illustrated in the following section. Also, the direction from which beam radiation is received and its angle of incidence on various surface over any time span will be analyzed. Then, the last part of the following section is provided to describe the modeling used to estimate the total solar radiation on horizontal and tilt surface.

2.1. Sun–earth geometric relationships and incidence angle

The geometric relationships between a plane of any particular orientation relative to the earth at any time and the beam solar radiation can be described by appropriate relationships in term of several angles [33] illustrated in Fig. 1.

2.1.1. True and mean anomaly of the earth

The true anomaly is an angular parameter that defines the position of the earth moving along a Keplerian orbit. It is the angle between the direction of the periapsis and the current position of the earth as seen from the sun [45].

The mean anomaly B, called also the fractional year, is a parameter relating position and time for the earth moving in a Kepler orbit. It is what the true anomaly would be if the earth moved with constant speed along a perfectly circular orbit around the sun in the same time.

The mean anomaly B is given by the following formula:

$$B = \frac{360(n-1)}{365} \tag{1}$$

where n is the ordinal date. $n=1$ at January 1st and $n=365$ at December 31st.

2.1.2. Earth obliquity and sun declination

The earth obliquity, also called earth axial tilt, is the angle between its rotational axis, and a perpendicular to the orbital plane. The tilt and direction of the rotational axis with respect to the orbit change very slowly (over thousands of years) [46]. The actual value of obliquity is 23.45° [47].

The declination of the sun δ is the angle between the rays of the sun and the plane of the earth's equator. Solar declination varies with the seasons and its period is one year. At the solstices, δ reaches its maximum value of 23.45°′. Therefore δ = +23.45° at the summer solstice while δ = −23.45° at the winter summer solstice. At the equinoxes, δ is equal to 0°.

In term of the mean anomaly B, the declination is given by [48]:

$$\begin{aligned}\delta = {} & 0.006918 - 0.3999912\ \cos B + 0.070257 \sin B \\ & - 0.006758 \cos 2B + 0.0000907 \sin 2B \\ & - 0.002679 \cos 3B + 0.00148 \sin 3B\end{aligned} \tag{2}$$

In term of ordinal date, the declination is expressed by the following formula [49]:

$$\delta = 23.45^\circ\ \sin\left(360 \frac{284+n}{365}\right) \tag{3}$$

2.1.3. Equation of time

The equation of time is the difference between mean time (time based on the average motion of a fictional sun which moves at a uniform rate) and true time (time based on a non-uniform motion of the physical sun around the earth). The true sun's apparent motion varies due to the elliptical nature of the earth's orbit and the inclination of the axis of the earth's rotation. It is calculated using the following expression:

$$\begin{aligned}E = {} & 3.8210^{-6}(75 + 1868\ \cos B - 32077 \sin B \\ & - 14619 \cos 2B - 40890 \sin 2B)\end{aligned} \tag{4}$$

2.1.4. Latitude and longitude

The latitude, φ, is the angular location north or south of the equator, north positive; $-90^\circ \le \varphi \le 90+$.

The longitude λ is a geographic coordinate that specifies the east–west position of a point on the Earth's surface. φ and λ are angular measurements, usually expressed in degrees, minutes and seconds.

2.1.5. Solar time and hour angle

Standard time zone is defined by geometrically subdividing the earth's spheroid into 24 lunes, bordered by meridians each 15°. Time zones are based on Greenwich Mean Time (GMT), the mean solar time at longitude 0° (the Prime meridian). Thus, to convert civil time, t_C, to solar time t_S, two corrections should be applied. The first one is the correction for the difference in longitude between the observer's meridian and the meridian on which the civil time is based. The second correction is from the equation of time (4). Solar time is expressed as follows:

$$t_S = t_C + \frac{\lambda}{15} - Z_C + E \tag{5}$$

where Z_C is the time zone east of GMT.

The hour angle ω is the solar angular displacement east or west of the local meridian due to the rotation of the earth (15° per hour). The hour angle is negative in the morning and positive afternoon. Therefore, the hour angle can be written as follows:

$$\omega = (t_S - 12) \cdot 15^\circ \tag{6}$$

2.1.6. Zenith, solar altitude and azimuth angles

The zenith angle θ_z is defined as the angle between the vertical and the line to the sun, which is, the angle of incidence of a beam radiation on a horizontal plane. The zenith angle is expressed in terms of latitude φ, declination δ and hour angle, ω as follows:

$$\cos\ \theta_z = \cos\varphi\cos\delta\cos\omega + \sin\varphi\sin\delta \quad (7)$$

The solar altitude angle α_S is the angle between the horizontal and the line to the sun, that is, the complement of the zenith angle.

The solar azimuth angle γ_S is defined as the angular displacement from south of the projection of beam radiation on horizontal plane, with zero due south, east negative, west positive; $-180^\circ \le \gamma \le 180^\circ$.

2.1.7. Surface azimuth and slope angles

The surface azimuth angle γ is the deviation of the projection on a horizontal plane of the normal to the surface from the local meridian. The slope, β, referred also to the surface inclination, is the angle between the plane of the surface in question and the horizontal; $0^\circ \le \beta \le 180$.

2.1.8. Angle of incidence

The incidence angle θ is the angle between the beam radiation and the normal to the surface with any orientation. It can be expressed using the following equation [33]:

$$\begin{aligned}\cos\ \theta &= \sin\varphi\sin\delta\cos\beta \\ &\quad - \cos\varphi\sin\delta\sin\beta\cos\gamma \\ &\quad + \cos\varphi\cos\delta\cos\beta\cos\omega \\ &\quad + \sin\varphi\cos\delta\sin\beta\cos\gamma\cos\omega \\ &\quad + \cos\delta\sin\beta\sin\gamma\sin\omega\end{aligned} \quad (8)$$

2.2. Extraterrestrial solar radiation

2.2.1. Solar constant

The solar constant, called also the extraterrestrial radiation, G_{sc} is defined as the energy from the sun per unit time received on a unit area of surface perpendicular to the direction of propagation of the radiation at mean earth–sun distance outside the atmosphere. In earlier works, the estimations and measurements of the extraterrestrial irradiance have re-examined many times. In fact, Johnson revised the Abbot's extraterrestrial irradiance value of 1322 W/m^2 to 1395 W/m^2 (1954) [50]. In 1971, the NASA and the American Society of Testing and Materials accepted the Thekaekara and Drummond [51], value of 1353 W/m^2. In 1978, Frohlich [52] recommended a new value of 1373 W/m^2. Wilson et al. reported 1368 W/m^2 as a new value in 1982. In this study, the 1367 W/m^2 value adopted by the World Radiation Center (WCR) is used.

2.2.2. Normal extraterrestrial radiation

The normal extraterrestrial radiation G_{on} is defined as the amount of solar radiation striking a surface normal to the sun's rays at the top of the earth's atmosphere. Spencer [48] provided an accurate equation of the normal extraterrestrial radiation as follows:

$$\begin{aligned}G_{on} &= G_{sc}(1.00011 + 0.034221\ \cos B + 1.0001280\sin B \\ &\quad + 0.000719\cos 2B + 0.000077\sin 2B\end{aligned} \quad (9)$$

The normal extraterrestrial radiation can be given by a simple adequate equation for most engineering calculations:

$$G_{on} = G_{sc}\left(1 + 0.033\ \cos\frac{360n}{365}\right) \quad (10)$$

2.2.3. The horizontal extraterrestrial radiation

The horizontal extraterrestrial radiation G_{oh} is the amount of solar radiation received by a horizontal surface at the top of atmosphere. The horizontal extraterrestrial radiation can be calculated basing on Eqs. (7) and (10) as follows:

$$G_{oh} = G_{on}\ \cos\theta_z \quad (11)$$

The average extraterrestrial horizontal radiation over a time step can be calculated as:

$$\bar{G}_{oh} = \frac{12}{\pi}G_{on}\left[\cos\ \varphi\cos\delta(\sin\omega_2 - \sin\omega_1) + \pi\frac{(\omega_2 - \omega_1)}{180}\sin\varphi\sin\delta\right] \quad (12)$$

where ω_1 and ω_2 are respectively the hour angle at the beginning of the time step and the hour angle at the end of the time step.

2.3. Radiation on horizontal surface

2.3.1. Global radiation

The global radiation, $\bar{G}$ on horizontal plane, is the sum of diffuse radiation $\bar{G}_d$ and the direct radiation $\bar{G}_b$. It is expressed as follows:

$$\bar{G} = \bar{G}_b + \bar{G}_d \quad (13)$$

2.3.2. Diffuse radiation

The diffuse radiation $\bar{G}_d$ is solar reaching the earth's surface after having been scattered from the direct solar beam by molecules or suspensoids in the atmosphere [53].

The clearness index factor K is defined as the ratio of a particular global radiation to the horizontal extraterrestrial radiation:

$$K = \frac{\bar{G}}{\bar{G}_{oh}} \quad (14)$$

Basing on the data from four U.S. and one Australian station and using the clearness index K, Erbs et al. [54] (1982) suggested a correlation to resolve global radiation into its beam and diffuse components:

$$\frac{\bar{G}_d}{\bar{G}} = \begin{cases} 1.0 - 0.09K \\ (\text{for } K \le 0.22) \\ 0.9511 - 0.1604K + 4.388K^2 - 16.638K^3 + 12.336K^4 \\ (\text{for } 0.22 \le K \le 0.8) \\ 0.165 \\ (\text{for } K > 0.8) \end{cases} \quad (15)$$

Furthermore, Reindl et al. [55] (1979) proposed another correlation as follows:

$$\frac{\bar{G}_d}{\bar{G}} = \begin{cases} 1.0 - 0.258K \\ (\text{for } K \le 0.3) \\ 1.45 - 1.67K \\ (\text{for } 0.3 \le K \le 0.78) \\ 0.147 \\ (\text{for } K > 0.78) \end{cases} \quad (16)$$

Moreover, Mondol et al. [56] (2008) suggested the following correlation:

$$\frac{\bar{G}_d}{\bar{G}} = \begin{cases} 0.98K \\ (\text{for } K \le 0.2) \\ 0.61092 + 3.6259K - 10.171K^2 + 6.388K^3 \\ (\text{for } 0.22 \le K \le 0.8) \\ 0.672 - 0.474K \\ (\text{for } K > 0.8) \end{cases} \quad (17)$$

2.3.3. Beam radiation

The beam radiation, $\bar{G}_b$ is defined as solar radiation that travels from the sun to the earth's surface without any scattering by the atmosphere. In this study, the correlation proposed by Erbs et al.

[54] will be used to estimate the diffuse radiation $\bar{G}_d$ and then the beam radiation $\bar{G}_b$ is calculated by subtracting the diffuse radiation from the global horizontal radiation.

2.4. Radiation on inclined surface

Many authors presented a several models in order to convert the solar radiations for a horizontal surface to that for a tilted one. These models use the same method of calculating beam and ground reflected radiation on a tilted surface and the only difference exists in the treatment of the diffuse radiation [53].

2.4.1. Beam radiation

The beam radiation on tilted surface, $\bar{G}_{bt}$, can be estimated by multiplying its value on a horizontal surface, $\bar{G}_b$, by a geometric factor R_b which depends on the zenith and incidence angles. R_b is given by the following the expression [33,57,58]:

$$R_b = \frac{\cos\,\theta}{\cos\theta_z} \tag{18}$$

Thus, the beam radiation on tilted surface $\bar{G}_{bt}$ is expressed as:

$$\bar{G}_{bt} = \bar{G}_b \times R_b = \bar{G}_b \times \frac{\cos\,\theta}{\cos\theta_z} \tag{19}$$

2.4.2. Diffuse radiation

As mentioned previously, the only difference among the models appears in the assessment of sky-diffuse component [59–64].

It has been pointed out that the sky diffuse component is considered to be the largest potential source of computational error [65,66]. In fact, the most complex problem of estimating the diffuse irradiance on tilted surface, $\bar{G}_{dt}$, is related to the fact that this diffuse component does not have an isotropic distribution in the sky and this distribution is not uniform over the time. Many authors investigated the diffuse radiation component basing on various measurements from several stations. In order to evaluate this component, they used many models classified basically on three types: isotropic, circum-solar and anisotropic.

2.4.2.1. Isotropic models. The isotropic models presume that the intensity of diffuse radiation is uniform over the entire hemisphere sky dome which could be true in the case of overcast skies. Hence, the diffuse radiation incident on a tilted surface depends on the fraction of the sky dome seen by it [53].

Later, Dorota [67] revealed that many models calculating solar radiation on an inclined surface of any particular orientation have been performed and the isotropic diffuse sky model, Hottel–Woertz–Liu–Jordan [68,69], is the most used. According to this model diffuse component is given as follows:

$$\bar{G}_{dt} = \bar{G}_d \times \left(\frac{1+\cos\,\beta}{2}\right) \tag{20}$$

where β is the slope of the considered surface.

However, despite the popularity of the isotropic models, theoretical as well as experimental results have shown that the simplified calculations of isotropic model do not give a real picture of the isolation conditions [67]. In fact, they showed the poorest performance and should not be used for estimating the diffuse radiation on a tilted surface [55].

2.4.2.2. Circum-solar models. The circum-solar model presumes that all the radiation comes from the direction of the sun and its surroundings, and, therefore, that the diffuse component is calculated analogously to the direct component [33,57]:

$$\bar{G}_{dt} = \bar{G}_d \times R_b \tag{21}$$

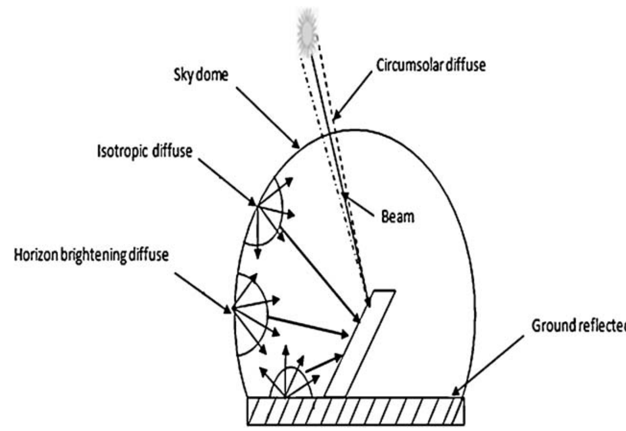


Fig. 2. Schematic view of the solar radiation distribution on a tilted surface according to anisotropic diffuse sky model.

Unfortunately, this model could only be applied in the case of completely clear skies, generally overestimates the diffuse component of the radiation [57].

2.4.2.3. Anisotropic models. The anisotropic model assume the anisotropy of the diffuse sky radiation in the circumsolar region (sky near the solar disc) and the isotropy diffuse component distribution from the rest of the sky dome. This model is widely accepted, it is used both for clear and cloudy or partly cloudy days [57]. Based on the above, an important number of models considering anisotropic distribution of the diffuse irradiance in the sky are proposed [70–74]. In this context, one of the most confirmed anisotropic sky model is the HDKR, Hay–Davies–Klucher–Reindl, model [67]. This model assumes that there are three components to the diffuse solar radiation: an isotropic component which comes from all parts of the sky equally, a circumsolar diffuse component which is concentrated in the sky near the sun and a horizon brightening component which emanates from the sky near the horizon (Fig. 2).

According to The HDKR model the diffuse component radiation incident on a tilted surface is as follows:

$$\bar{G}_{dt} = \bar{G}_d(R_b A_i) + (1-A_i)\left(\frac{1+\cos\beta}{2}\right)\left[1+f\sin^3\left(\frac{\beta}{2}\right)\right] \tag{22}$$

where the factor f accounts the fact that more diffuse radiation comes from the horizon than from the rest of the sky, this modulating correction factor of diffuse radiation includes influence of cloudiness and it is expressed by:

$$f = \sqrt{\frac{\bar{G}_b}{\bar{G}}} \tag{23}$$

A_i, is the anisotropy index used to estimate the amount of circumsolar diffuse radiation, also called forward scattered radiation. This factor is expressed as a ratio of beam radiation on a horizontal ground surface to extraterrestrial radiation. Its high value enhances the contribution of circumsolar diffuse radiation. The anisotropy index is given by:

$$A_i = \frac{\bar{G}_b}{\bar{G}_o} \tag{24}$$

2.4.3. Ground reflected radiation

All models assume that the ground reflected component is isotropic as follows [49,57,58,75]:

$$\bar{G}_r = \bar{G} \times \rho \times \left(\frac{1-\cos\,\beta}{2}\right) \tag{25}$$

where ρ is the albedo coefficient of the ground.

2.4.4. Global radiation

The global radiation on a tilted surface, $\bar{G}_t$, is the sum of the diffuse radiation, $\bar{G}_{dt}$, beam radiation $\bar{G}_{bt}$, and the ground reflected radiation, $\bar{G}_r$. Therefore, the incident global radiation on tilted surface is given by the following expression [76–81]:

$$\bar{G}_t = \bar{G}_{bt} + \bar{G}_{dt} + \bar{G}_r \quad (26)$$

In this study, the HDKR model will be applied assuming that the global radiation on tilted surface is:

$$\bar{G}_t = (\bar{G}_b + \bar{G}_d A_i)R_b + \bar{G}_d(1 - A_i)R_d \left[1 + f \sin^3\left(\frac{\beta}{2}\right)\right] + \bar{G}\rho_g R_r \quad (27)$$

3. PV generation

The PV generation is mainly dependent on the global incident radiation (which was overviewed in the previous section) and the PV cell temperature.

3.1. PV cell temperature

It is well known that the PV cell temperature has an important effect on the PV output power. This temperature can be the same as the ambient temperature during the night but it can go over the ambient temperature by 30° or more in full sun. Hence, it is necessary to calculate the PV cell temperature in order to account for this meaning effect. For this reason, we have to begin by establishing the energy balance between, on one hand, the solar energy absorbed by the PV array, and on the other hand, the electrical output plus the heat transfer to the surroundings. The balance on unit area of the module which cooled by losses to the surroundings can be written as [33]:

$$\tau\alpha G_T = \eta_C G_T + U_L(T_C - T_a) \quad (28)$$

where $\tau, \alpha, G_T, \eta_C, U_L$ and T_a are respectively the solar transmittance of the PV array, the solar absorptance of the PV array, the global radiation striking the PV array, the electrical conversion efficiency of the PV array, the coefficient of heat transfer to the surroundings and the ambient temperature.

According to the above equation, the PV cell temperature can be expressed as follows:

$$T_C = T_a + G_T\left(\frac{\tau\alpha}{U_L}\right)\left(1 - \frac{\eta_C}{\tau\alpha}\right) \quad (29)$$

To estimate the value of $(\tau\alpha/U_L)$, we report the nominal operating cell temperature (NOCT), which is defined as the cell temperature that results at an incident radiation of 0.8 kW/m^2, an ambient temperature of 20 °C, and no load operation (meaning $\eta_C = 0$), average wind speed equal to 1 m/s [82,83]. We can substitute these values into the above equation and solve it for $(\tau\alpha/U_L)$:

$$\frac{\tau\alpha}{U_L} = \frac{T_{C,\mathrm{NOCT}} - T_{a,\mathrm{NOCT}}}{G_{T,\mathrm{NOCT}}} \quad (30)$$

where $T_{C,\mathrm{NOCT}}$, $T_{a,\mathrm{NOCT}}$ and $G_{T,\mathrm{NOCT}}$ are respectively the nominal operating cell temperature, the ambient temperature and the solar radiation at which the NOCT is defined.

If we presume that $(\tau\alpha/U_L)$ is constant, we can substitute this equation into the cell temperature equation as follows:

$$T_C = T_a + G_T\left(\frac{(T_{C,\mathrm{NOCT}} - T_{a,\mathrm{NOCT}})}{G_{T,\mathrm{NOCT}}}\right)\left(1 - \frac{\eta_C}{\tau\alpha}\right) \quad (31)$$

We suppose that the PV array always operates at its maximum power point, which means that the cell efficiency is always equal to the maximum power point efficiency η_{mp}:

$$\eta_C = \eta_{mp} \quad (32)$$

In this order, we can substitute η_C by η_{mp} in the relation (31) which can be written therefore as follows [84]:

$$T_C = T_a + (T_{C,\mathrm{NOCT}} - T_{a,\mathrm{NOCT}})\left(\frac{G_T}{G_{T,\mathrm{NOCT}}}\right)\left(1 - \frac{\eta_{mp}}{\tau\alpha}\right) \quad (33)$$

However, η_{mp} depends on the cell temperature T_C, we can assume that the efficiency varies linearly with temperature according to the following equation:

$$\eta_{mp} = \eta_{mp,stc}[1 + \alpha_P(T_C - T_{C,stc})] \quad (34)$$

where η_{mp}, α_P and $T_{C,stc}$ are respectively the maximum power point efficiency under standard test conditions (a radiation of 1 kW/m^2, a cell temperature of 25 °C, and no wind), the temperature coefficient of power and the cell temperature under standard test conditions. We note here that the temperature coefficient of power (α_P) is negative which means that the efficiency of the PV array decreases with increasing cell temperature.

Finally, by substituting this efficiency equation (34) into the above cell temperature equation (33), the cell temperature becomes:

$$T_C = \frac{T_a + (T_{C,\mathrm{NOCT}} - T_{a,\mathrm{NOCT}})(G_S/G_{S,\mathrm{NOCT}})[1 - (\eta_{mp,stc}/\tau\alpha)(1 - JT_{C,stc})]}{1 + (T_{C,\mathrm{NOCT}} - T_{a,\mathrm{NOCT}})(G_S/G_{S,\mathrm{NOCT}})(J\eta_{mp,stc}/\tau\alpha)} \quad (35)$$

3.2. PV output power

The assessment of the PV output power was the interest of many authors. Thus, a several models [85] have been developed in order to evaluate all PV characteristics. In fact, Osterwald [86] suggested a method to calculate the power provided by a photovoltaic generator. This method assumes that:

$$P_m = P_{m,stc}\left(\frac{\bar{G}_T}{\bar{G}_{T,stc}}\right)[1 - \alpha_P(T_C - T_{C,stc})] \quad (36)$$

where P_m and $P_{m,stc}$ are respectively the cell maximum power and the cell maximum power in the standard test conditions.

Green and Araujo et al. [87,88] described another method to calculate the output power of a PV module as follows:

$$P_m = V_{oc} \times I_{sc} \times (1 - a^{-b})\left[1 - \frac{b}{\vartheta_{oc}} \times \ln(a) - r_s \times (1 - a^{-b})\right] \quad (37)$$

where V_{oc}: cell open circuit voltage; I_{sc}: cell short circuit current; ϑ_{oc}: standard cell voltage; r_S: standard resistance; a: $\vartheta_{oc} + 1 - 2(\vartheta_{oc} \times r_s)$; $b : a/(1 + a)$.

Araujo et al. [88] used the diode model to calculate the operation values of a PV generator. This model defines the *V–I* characteristic of the PV generator as follow:

$$I_G = N_{mp}N_{cp}I_{sc}\left[1 - \exp\left[\frac{V_G/(N_{cs}N_{ms}) - V_{oc} + I_G \cdot R_s/(N_{cp}N_{mp}}{V_t}\right]\right] \quad (38)$$

where I_G: PV generator current (A); V_G: PV generator voltage (V); N_{cp}: parallel cells number of PV module; N_{cs}: parallel modules number of PV generator; N_{mp}: parallel modules number of PV generator; N_{ms}: series modules number of PV generator; R_s: series resistance of a photovoltaic cell module (Ω); V_t: thermal voltage (V).

In this study, we will use one of the simplest model to predict the PV array output power which assumes that:

$$P_{PV} = Y_{PV}f_{PV}\left(\frac{\bar{G}_T}{\bar{G}_{T,stc}}\right)\left[1 + \alpha_P(T_C - T_{C,stc})\right] \quad (39)$$

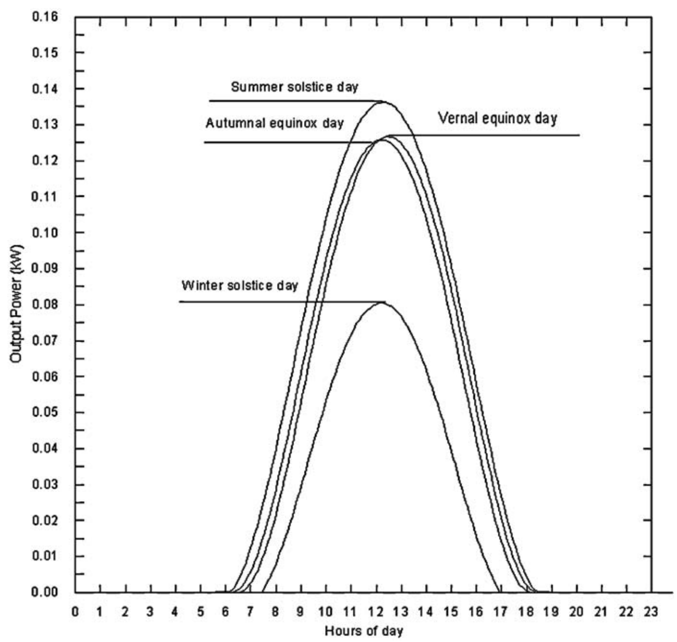


Fig. 3. Instantaneous PV output power ($\beta = 36^\circ$, $\gamma = 0^\circ$) during the different equinox and solstice days.

where Y_{PV}, f_{PV}, $\bar{G}_{T,stc}$, α_P, T_C and $T_{C,stc}$ are respectively the rated capacity of the PV array, meaning its power output under standard test conditions, the PV derating factor (it is used to account for such factors as shading, snow cover, aging, and so forth), the incident radiation at standard test conditions, the temperature coefficient of power (which indicates how strongly the PV array power output depends on the cell temperature), the PV cell temperature in the current time step and finally the PV cell temperature under standard test conditions.

4. Outcome results

This study is related to the Monastir city which is situated on the central coast of Tunisia, in the Sahel area (20 km south of Sousse and 162 km south of Tunis). The latitude and longitude of this town are respectively 36°N and 12°E and an altitude of 10 m above sea level. Despite of meteorological data lack, we have used the same level of clearness index for all studied cases ($K = 1$) basing on the Erbs et al. [54] clearness index correlation. It should be noted also that all simulations in this work are computed with a time step equal to ((1/10) h).

4.1. Effect of date on the instantaneous PV output power

In order to study the dependence of the photovoltaic production with the effect of date throughout the whole year, four extreme days of the year are considered, i.e. vernal and autumnal equinox, and summer and winter solstice days. The results are carried out for a PV module oriented straight to the south by 0° Azimuth angle as well as a tilt angle equal to the latitude of Monastir (36°).

The simulated results in terms of instantaneous PV output power for the abovementioned dates are illustrated in Fig. 3. Due to the difference in the length of the day between summer and winter, one can observe that the PV panel is generating electricity slightly for less than 10 h at the winter solstice day and to slightly for more than 12 h at the summer solstice day. During the day, the PV output power will begin to increase from sunrise to midday then decline until sunset. It is worth noting that the PV output power maximums registered at midday differ from date to another. This can be related to how high in the sky the sun appears. The operating hours of PV system in winter is shorter than in spring (or autumn) because the short sunshine time in winter compared to the vernal or autumn periods. This phenomenon was observed also by other researchers such as Chang [75] who found that in the northern hemisphere, the sun's elevation angle during winter (November, December, and January) is lower than during the other seasons. This is because the mean distance between the Earth and the Sun in winter is less than that in spring (or autumn) by about 3% due to the eccentricity of the Earth's orbit, resulting in a stronger flux of radiation.

4.2. Effect of tilt angle on the instantaneous PV output power

One of the important parameters that affect the performance of a PV system is its tilt angle with the horizontal. This is due to the fact that the variation of tilt angle changes the amount of solar radiation reaching the PV panel.

Fig. 4 shows the instantaneous PV output power for different inclinations in Monastir during the four mentioned days (the winter solstice, the summer solstice, the vernal equinox and the autumnal equinox day).

It is observed that the tilt angle has a very significant effect on the instantaneous photovoltaic production during the summer solstice day relatively compared to the effect during the winter solstice day, near the results of Hussein et al. [38]. This is because the zenith angle of the sun varies from 90° at the sunrise and the sunset to slightly more than 0° at the midday in the summer season while it varies only from 90° to slightly less than 60° in the winter season. Thus, for a tilt angle equal 36°, the variation of solar radiation incident angle on the PV array is more important in summer days than in winter days. That's why in the summer solstice day, the maximum PV output power varies from less than 60 W for an inclination angle equal to 90° to more than 140 W for an inclination angle equal to 15° while in the winter solstice day, it varies only from more than 40 W for an inclination angle equal to 0° to less than 90 W for an inclination angle equal to 60°. In the two equinox days, the maximum PV output power varies from more than 90 W for an inclination angle equal to 90° to less than 130 W for an inclination angle equal to 45°.

4.3. Monthly optimal tilt angles for a south facing panel

In order to enhance the PV output power of a module without tracking system, Gunerhan and Hepbasli [41] recommends that solar collector systems have to be adjusted with the optimal angle every month. Table 1 recapitulates the monthly optimal tilt angle for a PV module mounted facing the south in the Monastir city. Theses angles vary from 4° in June to 65° in December. The variation of the optimal monthly tilt angle during the year is shown in Fig. 5. It is observed that in the first six months, the optimal tilt angle has the trend to decrease from 63° in January to 4° in June. However, in the second half of the year the optimal tilt angle witness a progress till 65° at the end of the year. This monthly optimal tilt angle tendency is in good agreement with the results of many researchers [33,41,53]. One can deduce that this variation has the same trend as the variation of the zenith angle of the sun during the year. In Monastir city and in other mid-latitude countries north of the equator, the sun's daily trip is an arc across the southern sky. The sun's greatest height above the horizon occurs at noon, and how high the sun then gets depends on the season of the year, it is the highest in mid-summer (June), which correspond to the lowest zenith angle value, the lowest in mid-winter (December) that correspond to the highest zenith angle value. This phenomenon was concluded also by Kelly and Gibson [89] in term of altitude angle. Indeed, they found that for the winter solstice day, the maximum altitude angle

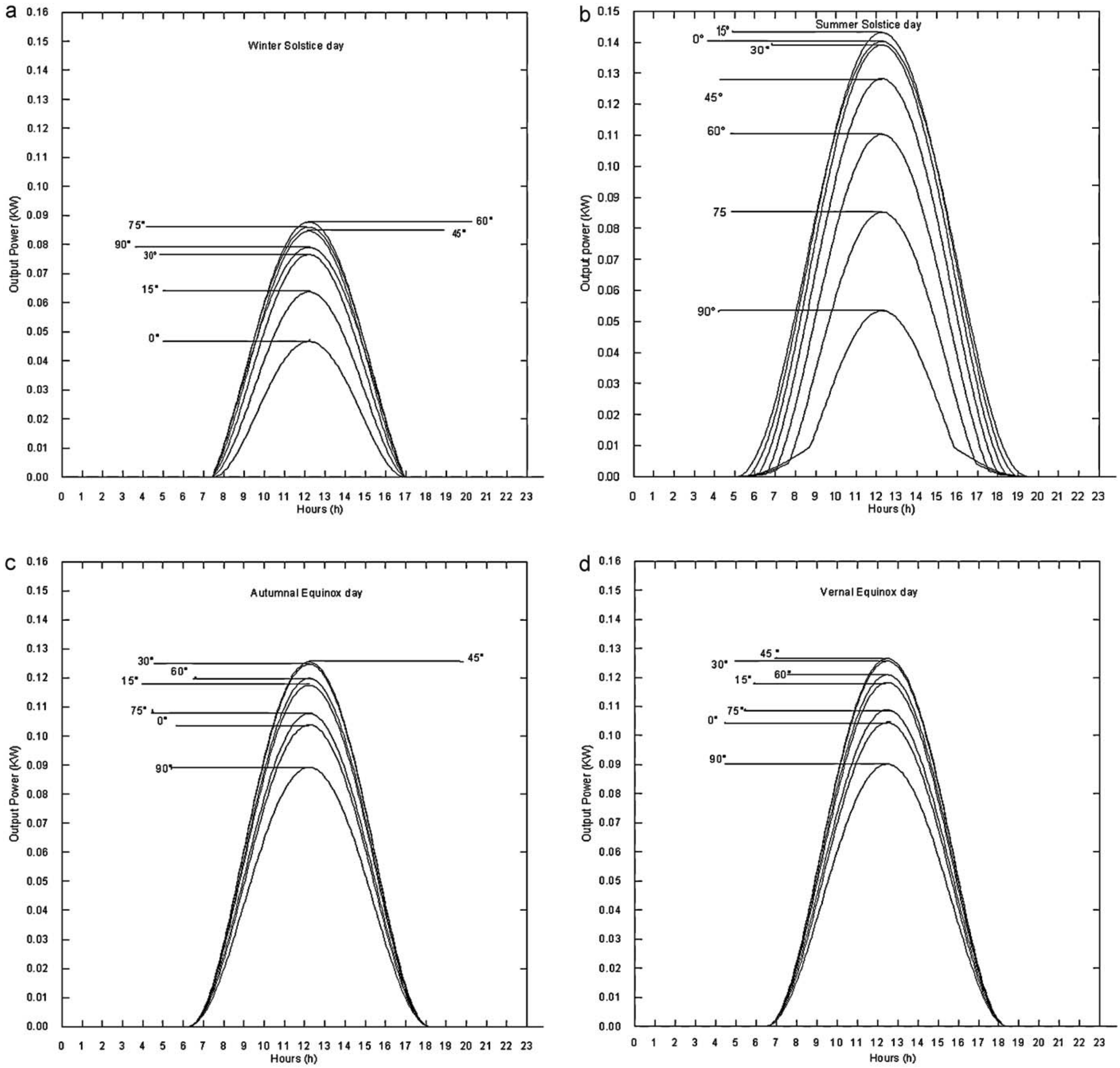


Fig. 4. Instantaneous PV output power in terms of different inclinations during winter solstice (a), summer solstice (b), autumnal equinox (c) and vernal equinox (d) days.

is $\alpha = 24.2^{\circ}$ while for the summer solstice day, the maximum solar altitude angle is $\alpha = 71.1^{\circ}$.

4.4. Yearly tilt angle for a south facing panel

Unfortunately, the cost of a monthly tracked PV System prohibits the use of this technology for many applications. This inconvenience can be solved by finding out, with precision, the yearly optimal tilt angle for a fixed PV module.

Fig. 6 shows the yearly Output Energy at different tilt angles. For a horizontal PV Surface, the computed output energy is equal to 234 kWh/year while for a vertical PV surface mounted to the south face the computed output energy is less than 167 kWh/year. It is found that the maximum of the yearly output energy can be obtained with a tilt angle equal to 33° which is close to 0.9 times latitude of Monastir city. This result is in good agreement with the simulation result of Chang [58] who predicted that the yearly optimal tilt angle, for a south-facing fixed panel, for latitudes below 65° in the northern hemisphere is equal to 0.9 latitude. For this angle,

Table 1
Monthly optimal tilt angles.

Month	January	February	March	April	May	June	July	August	September	October	November	December
Optimal slope	63°	55°	42°	25°	11°	4°	7°	19°	34°	51°	61°	65°

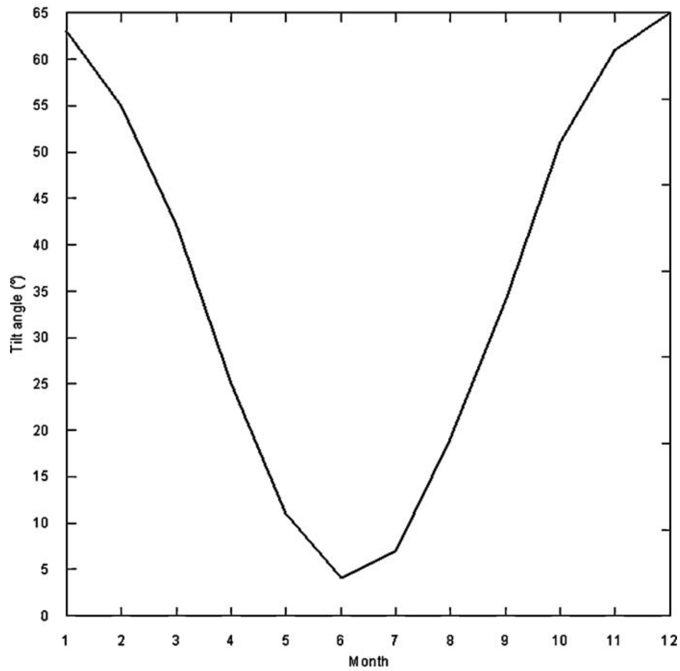


Fig. 5. Monthly optimal tilt angles for a facing south panel.

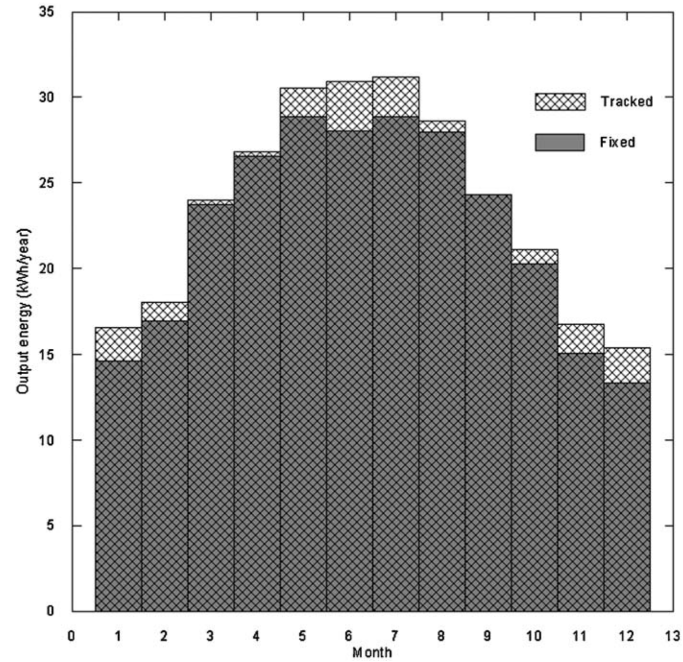


Fig. 7. Monthly PV output power generated by a traditional fixed and a single-axis tracked panel.

the output energy can reach more than 268 kWh/year. However, for fixed PV using this value of tilt angle the energy produced in summer is not the maximum since it is calculated for the whole year and not for only the summer season.

4.5. Comparison between the output power generated by a traditional fixed and single-axis tracked panel

A comparison of monthly output energy between fixed and tracked southern face mounted PV module is illustrated in Fig. 7. It is noticed that the optimal yearly tilt angle computed below (i.e. 33°) is used for the fixed panel and the optimal monthly tilt angles are used for the tracked system. One can observe that the tracked panel generates stronger output energy than a traditionally fixed panel due to its smaller incidence angle of sunlight.

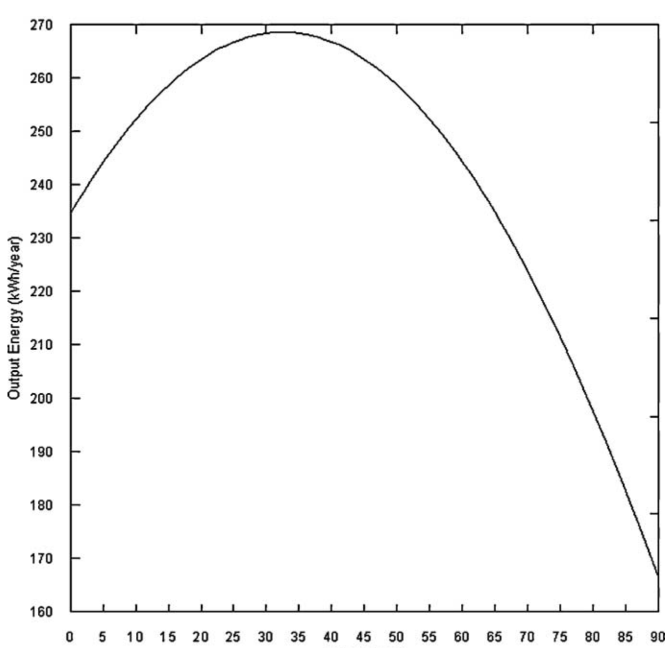


Fig. 6. Yearly optimal tilt angle for a facing south panel.

The monthly increment of output energy obtained by the tracked panel is marked with black color. One can observe that the gain provided by the tracked panel is more noticeable for tow critical periods. The first period corresponds to the months of May, June and July and the second period corresponds to November, December and January months. The first period correspond to the summer solstice at June, in which the gain reveals its highest value equal to 2.9 kWh corresponding to 10.34% of energy generated by a fixed PV collector. The second period marked by the occurrence of the winter solstice at December. During this period, the gains made by the tracked panel relative to a fixed panel reach, in December, more than 15% corresponding to 2.06 kWh. Throughout the other months, the gain reaches only a value slightly more than 1 kWh in the month of February. Table 2 lists the Output power of PV and gains for different time periods. This variation of Gain can be explained by the fact that in summer and winter solstices the solar zenith angles reach respectively their lowest and highest values so the incidence angle of solar rays on fixed panel is more important at these periods. The yearly accumulation gain made by the tracked panel relative to a fixed panel is evaluated to 15.48 kWh which correspond to 5.76%. This result was concluded by many other researchers. For instance, Lubitz [49] found that the gain made by tilt PV tracker across the contiguous United States of America with a value of 5% Neville. Tomson [90] described mainly the performance of PV modules with daily two-position in the morning and in the afternoon. His results indicated that the seasonal energy yield was increased by 10–20% over the yield from a fixed south facing collector tilted at an optimal angle.

4.6. Effect of azimuth angle on the instantaneous output power

When a module panel must be installed with the azimuth other than south, Fig. 8 illustrates the instantaneous output power for

Table 2
Output power of PV and gains for different time periods (kWh).

Month	January	February	March	April	May	June	July	August	September	October	November	December	Total
Fixed panel (kWh)	14.64	16.91	23.76	26.6	28.85	28.04	28.85	27.98	24.31	20.27	15.05	13.34	268.60
Tracked panel (kWh)	16.52	17.99	23.97	26.8	30.55	30.94	31.16	28.60	24.32	21.10	16.73	15.40	284.08
Gain (kWh)	1.88	1.08	0.21	0.20	1.70	2.90	2.31	062	0.01	0.83	1.68	2.06	15.48
Gain (%)	12.84	6.38	0.88	0.75	5.89	10.34	8.00	2.21	0.04	4.09	11.16	15.44	5.76

different azimuths respectively during summer and winter solstice days and autumnal and vernal equinox days. The panel, here, is installed with a constant tilt angle equal to the yearly optimal tilt angle (i.e. 33°) for the city of Monastir. In order to analyze the azimuth effect, many azimuth angles are investigated, i.e. −120°, −80°, −40°, 0°, 40°, 80°, and 120°. We remember that the azimuth angle due to the south is 0°, due east is −90°, due west is 90°, and due north is 180°. With fixed-azimuth systems, the panels are almost oriented towards the equator (0° azimuth in the northern hemisphere). One can observe that varying the azimuth angle

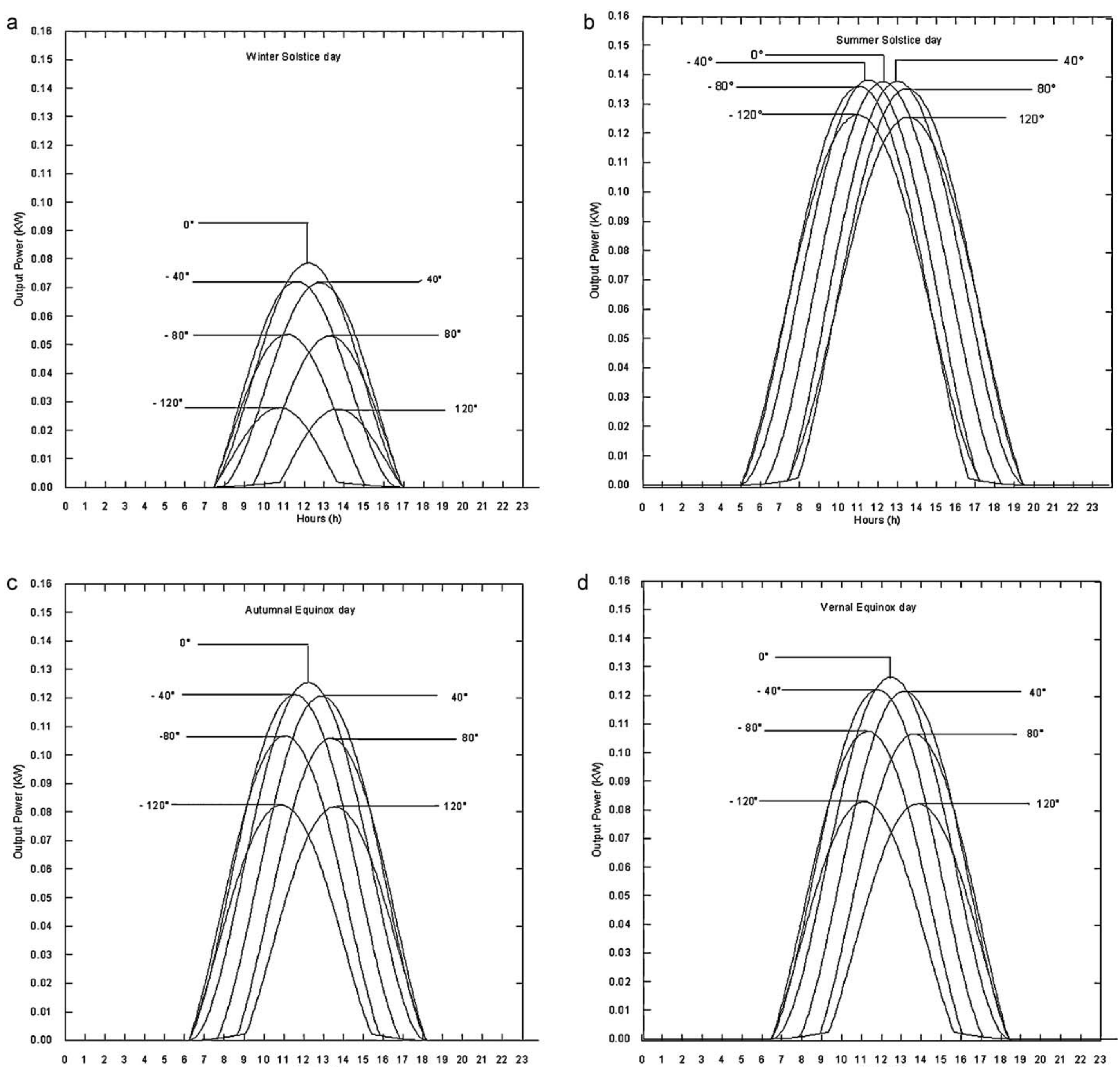


Fig. 8. Instantaneous PV output power in terms of different azimuth angles during winter solstice (a), summer solstice (b), autumnal equinox (c) and vernal equinox (d) days.

from −120° to 120° modify the position and the value reached by the maximum output power. For azimuth angle equal to 0° the peak of generated power is registered at the solar noon and it is the highest value relatively compared to the values reached for other azimuths. For negative values of the azimuth angles (east) the output power maximums are reached before the solar noon while for positive values of the azimuth angles (west) the output power maximums are reached after the solar noon. In summer solstice day, the maximum output power is recorded at 10h54′, 11h00′, 11h30′, 12h12′, 13h00′, 13h24′ and 13h30′ respectively for azimuth angles equal to −120°, −80°, −40°, 0°, 40°, 80° and 120°. Theses translations in time are accompanied by a decrease in term of the maximum output power values. In summer solstice day, this decrease is significant only for azimuth angles equal to −120° and 120° while in winter solstice day the decrease is significant for all considered azimuth angles. The decrease do not exceed 8.03% for azimuth angle equal to −120° or 120°, it is evaluated to 1.45% for azimuth angle equal to −80° or 80° and it is less than 0.01% for azimuth angle equal to −40° or 40° in summer solstice day while in winter solstice day this reduction achieve more than 65%, 32%, 7% respectively for azimuth angle equal to ±120°, to ±80°, to ±40°. For vernal and autumnal equinox days, the decrease is between 3.9% and 35% for azimuth angle between ±120° and ±40°. These results do not ignore the importance of installing PV panel facing a direction other than the south specially to cover a load at earlier or later hour. One can observe that for example in summer solstice day, the instantaneous output power for a PV panel with azimuth angle equal to 0° is evaluated only to 14 W and 4 W respectively at 7 h and 18 h and it can reach the values of 52 W and 34 W respectively at 7 h and 18 h with azimuth angles equal respectively to −120° and 120°. Hence, the gain made by choosing theses azimuth angles compared to the south direction is estimated to 271% and 750%.

4.7. Investigation of optimal tilt and azimuth angles

In the above analysis, we investigated separately the effect of tilt and azimuth angles on the instantaneous PV panel output power in the city of Monastir. In order to optimize the exploitation of PV installations, dual-axis tracked systems can be used. The first axe is a horizontal one to adjust the tilt angle, the second axe is a vertical one to adjust the azimuth angle. So the determination of a couple of optimal angles during the day has to be examined. Fig. 9 illustrates the variation of optimal tilt and azimuth angles of PV panel, in Monastir city, during four extreme days: winter and summer solstice days and autumnal and vernal equinox days. The results show that the optimal tilt angle is equal to 90° at the sunrise and at the sunset. A tilt angle equal to 90° corresponds to a vertical PV panel oriented to the sun at the horizon. In the first half of the day, this angle decrease from 90° until reaching the minimum at the solar noon, in the second half of the day it increases until 90° at the end of the day. This phenomenon was observed also by Chang [58] who showed that the optimal tilt angles of the tracked panel is 0° at noon, and increases towards dawn and dusk. The minimum reached by the optimal tilt angle at the solar noon varies from a day to another. Its highest value (i.e. 59°) is obtained for the winter solstice day and its lowest value (12°) is obtained for the summer solstice day. At any hour during the day, the optimal tilt angle for the summer solstice day is lower than the one for the winter solstice day. This is because in the winter season the sun zenith angle is more important than in the summer season. So the PV panel should be more inclined to be perpendicular to the sun rays. Besides, a tilt angle equal to 90° is suggested at 8 h and 17 h in the winter solstice day while this inclination is recommended before 7 h and after 19 h in the summer solstice day. This is related to the above stated fact that the day is longer in summer than in winter season.

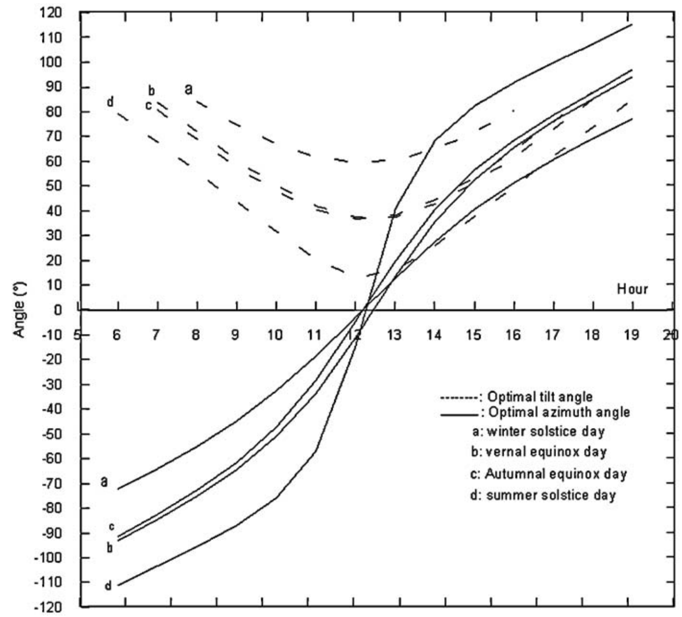


Fig. 9. Instantaneous optimal tilt and azimuth angles during winter solstice, summer solstice, autumnal equinox and vernal equinox days.

During the day, the optimal azimuth angle increases from negatives values corresponding to the east direction at the morning to positives values corresponding to the west direction. In the winter solstice day, it varies only from −70° to 70° wile in the summer solstice day it varies from less than −110° to more than 110°. This is explained by the same reasons mentioned above. One can observe that the variation rate of the optimal azimuth angles is more important between 10 h and 14 h. At this period surrounding the solar noon, the solar trajectory in the sky is perpendicular to the axe joining the PV panel to the sun. Thus the regular rotation of the earth (15°/h) corresponds to the highest displacement of the sun on its trajectory in the sky. This large displacement recommends a large variation of the azimuth angle.

4.8. Comparison between the output power generated by a traditional fixed and dual-axis tracked panel

Fig. 10 shows the instantaneous PV output power generated by fixed module with the yearly optimal tilt angle (i.e. 33°) facing due to the south and a dual axis tracked panel during the winter solstice (a), summer solstice (b), autumnal equinox (c) and vernal equinox (d) days, respectively, in Monastir city. It is found that the two-axis tracked panel produces stronger power than a traditionally fixed panel due to its optimal incidence angle of sunlight during the day. The same conclusion was proposed by Kacira et al. [91] who investigated the performance of PV modules mounted on a two-axis solar tracker. They concluded that the gain in the daily power generation could be 34.6%. The instantaneous increment of output power obtained by the dual-axis tracked panel is marked with black color. A similar gain was concluded by Tina and Gagliano using a two-axis tracked system in the site of Catania (Italy) [92]. The increment in term of PV produced energy made by the dual axis tracked PV system during the winter and summer solstice days reaches respectively 128 Wh and 413 Wh. Theses increments made by the dual-axis tracked PV system correspond to a gain of 30% and 44% respectively in the winter and summer solstice days relatively compared to a traditionally fixed panel.

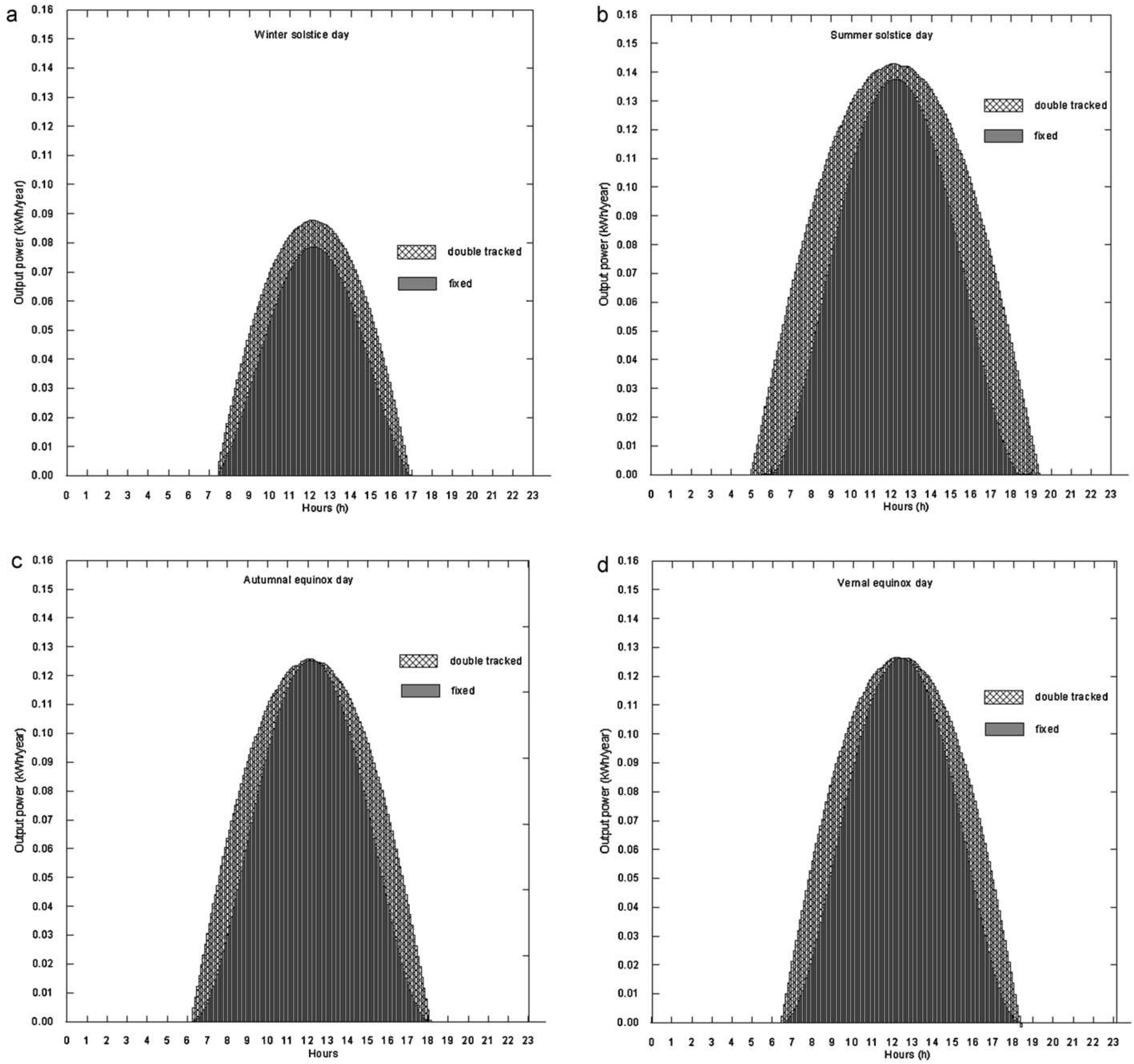


Fig. 10. Instantaneous PV output power generated by a traditional fixed and a dual-axis tracked panel during winter solstice (a) summer solstice (b), autumnal equinox (c) and vernal equinox (d) days.

5. Conclusion

An overview on research works on solar radiation basics and photovoltaic generation has been presented. Indeed, various models and approaches have been discussed to assess the total solar radiation on horizontal and tilt surface. Several methods for evaluating the output power of a PV module have been presented. A complete performance modeling and investigation of fixed, single and dual-axis tracking photovoltaic panel have been evaluated with details. These formulations are very useful for PV system assessment and planning for PV projects. Using the case study of Monastir, some concluding remarks are as follows:

- For Monastir city, the yearly optimal tilt angle of a fixed panel faced due to the south is close to 0.9 times the latitude.
- The gain made by the module mounted on a single-axis tracking panel relative to a traditional fixed panel are more noticeable for two critical periods which correspond to those surrounding the summer and the winter solstice dates. It reaches the value of 10.34% and 15% in the summer and winter solstice periods, respectively.
- The yearly gain made by a module mounted on a single-axis tracking system relative to a fixed panel installed with the yearly optimal tilt angle is estimated to 5.76%.
- In order to more optimize the solar systems exploitation, a dual-axis tracking installation can be used. The gains made by a dual-axis tracking panel relative to a traditional fixed panel are investigated. This gain reaches 30% and 44% respectively in the winter and summer solstice days.
- This study provide a guide to the choice of the optimal tilt and azimuths angles for fixed and tracked panel mounted on sin-

gle and dual-axis photovoltaic systems used in Monastir city (Tunisia).

References

[1] Mellit A, Kalogirou SA, Hontoria L, Shaari S. Artificial intelligence techniques for sizing photovoltaic systems: a review. Renewable and Sustainable Energy Reviews 2009;13:406–19.
[2] Meral ME, Dinc F. A review of the factors affecting operation and efficiency of photovoltaic based electricity generation systems. Renewable and Sustainable Energy Reviews 2011;15:2176–84.
[3] Pearce JM. Expanding photovoltaic penetration with residential distributed generation from hybrid solar photovoltaic and combined heat and power systems. Energy 2009;34:1947–54.
[4] Fthenakis VM, Alsema EA. Photovoltaics energy payback times, greenhouse gas emissions and external costs: 2004-early 2005 status. Progress in Photovoltaics: Research and Applications 2006;14:275–80.
[5] Pearce J, Lau A. Net energy analysis for sustainable energy production from silicon based solar cells. In: Cambell-Howe R, editor. Proc. of American Society of Mech. Engineers Solar 2002, Sunrise on the Reliable Energy Economy. 2002.
[6] Oliver M, Jackson T. Energy and economic evaluation of building-integrated photovoltaics. Energy 2001;26:431–9.
[7] Luque A, Hegedus S. Handbook of photovoltaic science and engineering. The Atrium, Southern Gate, Chichester, West Sussex, England: John Wiley & Sons Ltd.; 2003. p. 11–5.
[8] Joshi AS, Dincer I, Reddy BV. Performance analysis of photovoltaic systems: a review. Renewable and Sustainable Energy Reviews 2009;13:1884–97.
[9] Messenger RA, Ventre J. Photovoltaic system engineering. 2nd ed. Taylor & Francis e-Library; 2005. p. 15–6.
[10] Goetzberger A, Hoffmann VU. Photovoltaic solar energy generation. Berlin/Heidelberg, Germany: Springer-Verlag; 2005. p. 2.
[11] Patel MR. Wind and solar power systems. CRC Press LLC; 1999. p. 138.
[12] Posorski R. Photovoltaic water pumps, an attractive tool for rural drinking water supply. Solar Energy 1996;58:155–63.
[13] Reddy BS, Parikh JK. Economic and environmental impacts of demand side management programmes. Energy Policy 1997;25:349–56.
[14] Malaviya JN, Ranade SP. Potential of solar home-lighting system in rural western India. Solar Energy Materials and Solar Cells 1997;47:79–84.
[15] Bugaje IM. Remote area power supply in Nigeria: the prospects of solar energy. Renewable Energy 1999;18:491–500.
[16] Stutenbaumer U, Negash T, Abdi A. Performance of small-scale photovoltaic systems and their potential for rural electrification in Ethiopia. Renewable Energy 1999;18:35–48.
[17] Arab AH, Chenlo F, Mukadam K, Balenzategui JL. Performance of PV water pumping systems. Renewable Energy 1999;18:191–204.
[18] Meah K, Fletcher S, Ula S. Solar photovoltaic water pumping for remote locations. Renewable and Sustainable Energy Reviews 2008;12:472–87.
[19] Benatiallah A, Mostefaou R, Bradja K. Performance of photovoltaic solar system in Algeria. Desalination 2007;209:39–42.
[20] Hadi H, Tokuda S, Rahardjo S. Evaluation of performance of photovoltaic system with maximum power point (MPP). Solar Energy Materials & Solar Cells 2003;75:673–8.
[21] Sidrach-de-Cardona M, Mora Lopez L. Evaluation of a grid-connected photovoltaic system in southern Spain. Renewable Energy 1998;15:527–30.
[22] Chokmaviroj S, Wattanapong R, Suchart Y. Performance of a 500 kWP grid connected photovoltaic system at Mae Hong Son Province, Thailand. Renewable Energy 2006;31:19–28.
[23] Chaurey A, Kandpal TC. A review of the factors affecting operation and efficiency of photovoltaic based electricity generation systems. Renewable and Sustainable Energy Reviews 2011;15:2176–84.
[24] Hollmuller P, Joubert JM, Lachal B, Yvon K. Evaluation of a 5 kWp photovoltaic hydrogen production and storage installation for a residential home in Switzerland. International Journal of Hydrogen Energy 2000;25:97–109.
[25] Bilgen E. Solar hydrogen from photovoltaic-electrolyzer system. Energy Conversion and Management 2001;42:1047–57.
[26] Lehman PA, Chamberlin CE, Pauletto G, Rocheleau MA. Operating experience with a photovoltaic-hydrogen energy system. International Journal of Hydrogen Energy 1997;22:465–70.
[27] Tian W, Wan Y, Ren J, Zhu L. Effect of urban climate on building integrated photovoltaics performance. Energy Conversion and Management 2007;48:1–8.
[28] Wiser R, Bolinger M, Cappers P, Margolis R. Analyzing historical cost trends in California's market for customer-sited photovoltaics. Progress in Photovoltaic: Research and Applications 2007;15:69–85.
[29] Denholm P, Margolis RM. Evaluating the limits of solar photovoltaics (PV) in traditional electric power systems. Energy Policy 2007;35:2852–61.
[30] Tian PC. Output energy of a photovoltaic module mounted on a single-axis tracking system. Applied Energy 2009;86:2071–8.
[31] Tang R, Wu T. Optimal tilt-angles for solar collectors used in China. Applied Energy 2004;79:239–48.
[32] Li DHW, Lam TNT. Determining the optimum tilt angle and orientation for solar energy collection based on measured solar radiance data. International Journal of Photoenergy 2007. Article ID 85402, 9p.
[33] Duffie JA, Beckman WA. Solar engineering of thermal processes. New York: John Wiley and Sons; 1991.
[34] Al-Ismaily HA, Probert D. Photovoltaic electricity prospects in Oman. Applied Energy 1998;59:97–124.
[35] Shu N, Kameda N, Kishida Y, Sonoda H. Experimental and theoretical study on the optimal tilt angle of photovoltaic panels. Journal of Asian Architecture and Building Engineering 2006;5:399–405.
[36] Chen YM, Lee CH, Wu HC. Calculation of the optimum installation angle for fixed solar-cell panels based on the genetic algorithm and the simulated annealing method. IEEE Transactions on Energy Conversion 2005;20:467–73.
[37] Cheng CL, Charles S, Sanchez J, Meng-Chieh L. Research of BIPV optimal tilted angle, use of latitude concept for south orientated plans. Renewable Energy 2009;34:1644–50.
[38] Hussein HMS, Ahmad GE, El-Ghetany HH. Performance evaluation of photovoltaic modules at different tilt angles and orientations. Energy Conversion and Management 2004;45:2441–52.
[39] Chow TT, Chan ALS. Numerical study of desirable solar-collector orientations for the coastal region of South China. Applied Energy 2004;79:249–60.
[40] Shariah A, Al-Akhras MA, Al-Omari IA. Optimizing the tilt angle of solar collectors. Renewable Energy 2002;26:587–98.
[41] Gunerhan H, Hepbasli A. Determination of the optimum tilt angle of solar collectors for building applications. Building and Environment 2007;42: 779–83.
[42] Nijegorodov N, Devan KRS, Jain PK, Carlsson S. Atmospheric transmittance models and an analytical method to predict the optimum slope of an absorber plate, variously orientated at any latitude. Renewable Energy 1994;4:529–43.
[43] Yakup MABHM, Malik AQ. Optimum tilt angle and orientation for solar collector in Brunei Darussalam. Renewable Energy 2001;24:223–34.
[44] Kalogirou SA. Solar thermal collectors and applications. Progress in Energy and Combustion Science 2004;30:231–95.
[45] Murray CD, Demott SF. Solar dynamics. Cambridge University Press; 1999.
[46] Huybers P. Early Pleistocene Glacial Cycles and the Integrated Summer Insolation Forcing. Science 2006;313:508–11.
[47] Vyacheslav K, Ihor S. Introduction to solar motion geometry on the basis of a simple model. Physics Education 2010;45:641–53.
[48] Spencer JW. Fourier series representation of the position of the sun. Search 1971;2:172.
[49] Lubitz WD. Effect of manual tilt adjustments on incident irradiance on fixed and tracking solar panels. Applied Energy 2011;88:1710–9.
[50] Johnson FS. The solar constant. Journal of Meteorology 1954;6:431–9.
[51] Thekaekara MP, Drummond AJ. Standard values for the solar constant and its spectral components. Nature Physical Science 1979;229:6–9.
[52] Frohlich C. In: White OR, editor. Contemporary measures of the solar constant. In the solar output and its variation. Boulder: Colorado Associated University Press; 1977.
[53] Benghanem M. Optimization of tilt angle for solar panel: case study for Madinah, Saudi Arabia. Applied Energy 2011;88:1427–33.
[54] Erbs DG, Klein SA, Duffle JA. Estimation of the diffuse radiation fraction for hourly, daily, and monthly-average global. Solar Energy 1982;28:293–302.
[55] Reindl DT, Beckman WA, Duffie JA. Diffuse fraction corrections. Solar Energy 1990;45:1–7.
[56] Mondol JD, Yohanis YG, Norton B. Solar radiation modelling for the simulation of photovoltaic systems. Renewable Energy 2008;33:1109–20.
[57] Posadillo R, López LR. Evaluation of the performance of three diffuse hourly irradiation models on tilted surfaces according to the utilizability concept. Energy Conversion and Management 2009;50:2324–30.
[58] Chang TP. Output energy of a photovoltaic module mounted on a single-axis tracking system. Applied Energy 2009;86:2071–8.
[59] Díaz-Dorado E, Suarez-Garcia A, Carillo CJ, Cidràs J. Optimal distribution for photovoltaic solar trackers to minimize power losses caused by shadows. Renewable Energy 2011;36:1826–35.
[60] Berger W, Simon FG, Weimann K, Alsema EA. A novel approach for the recycling of thin film photovoltaic modules. Resources, Conservation and Recycling 2010;54:711–8.
[61] Syafaruddin, Karatepe E, Hiyama T. Polar coordinated fuzzy controller based real-time maximum-power point control of photovoltaic system. Renewable Energy 2009;34:2597–606.
[62] Kaldellis JK. Optimum technoeconomic energy autonomous photovoltaic solution for remote consumers throughout Greece. Energy Conversion and Management 2004;45:2745–60.
[63] Kim HS, Kim JK, Min BD, Yoo DW, Kim HJ. A highly efficient PV system using a series connection of DC–DC converter output with a photovoltaic panel. Renewable Energy 2009;34:2432–6.
[64] Abdolzadeh M, Ameri M. Improving the effectiveness of a photovoltaic water pumping system by spraying water over the front of photovoltaic cells. Renewable Energy 2009;34:91–6.
[65] Santamouris M, Tselepidaki I, Dris N. Evaluation of models to predict solar radiation on tilted surfaces for the Mediterranean region. Solar & Wind Technology 1990;7:585–9.
[66] Li DHW, Lam JC. Predicting solar irradiance on inclined surfaces using sky radiance data. Energy Conversion and Management 2004;45:1771–83.
[67] Dorota AC. Recommendation on modeling of solar energy incident on a building envelope. Renewable Energy 2009;34:736–41.
[68] Hottel HC, Woertz BB. Performance of flat plate solar heat collectors. Transactions of the ASME 1942;64:91.
[69] Liu BYH, Jordan RC. The long term average performance of flat-plate solar energy collectors: with design data for the US., its outlying possessions and Canada. Solar Energy 1963;7:53–74.

[70] Perez R, Seals R, Ineichen P, Steward R, Menicucci D. A new simplified version of the Perez diffuse irradiance model for tilted surfaces. Solar Energy 1987;39:221–32.
[71] Puri VM, Jiminer R, Menzer M, Costello FA. Total and non-isotropic diffuse insolution on tilted surfaces. Solar Energy 1980;25:85–90.
[72] Klucher TM. Evaluation of models to predict insolation on tilted surfaces. Solar Energy 1979;23:111–4.
[73] Temps RC, Coulson JL. Solar radiation incident upon slopes of different orientations. Solar Energy 1977;19:179–84.
[74] Gueymard C. An anisotropic solar irradiance model for tilted surfaces and its comparison with engineering selected algorithms. Solar Energy 1987;38:367–86.
[75] Chang TP. Performance evaluation for solar collectors in Taiwan. Energy 2009;34:32–40.
[76] Neville RC. Solar energy collector orientation and tracking mode. Solar Energy 1978;20:7–11.
[77] Morcos VH. Optimum tilt angle and orientation for solar collectors in Assiut, Egypt. Renewable Energy 1994;4:291–8.
[78] Al-Mohamad A. Efficiency improvements of photo-voltaic panels using a sun tracking system. Applied Energy 2004;79:345–54.
[79] Abdallah S. The effect of using sun tracking systems on the voltage–current characteristics and power generation of flat plate photovoltaics. Energy Conversion and Management 2004;45:1671–9.
[80] Huang BJ, Sun FS. Feasibility study of one axis three positions tracking solar PV with low concentration ratio reflector. Energy Conversion and Management 2007;48:1273–80.
[81] Sungur C. Multi-axes sun-tracking system with PLC control for photovoltaic panels in Turkey. Renewable Energy 2009;34:1119–25.
[82] Skoplaki E, Palyvos JA. On the temperature dependence of photovoltaic module electrical performance: a review of efficiency/power correlations. Solar Energy 2009;83:614–24.
[83] Stultz JN, Wen LC. Thermal performance testing and analysis of photovoltaic modules in natural sunlight. DOE/JPL LSA task report 1977:5101–31.
[84] Kou Q, Klein SA, Beckman WA. A method for estimating the long-term performance of direct-coupled PV pumping systems. Solar Energy 1998;64:33–40.
[85] Almonacid F, Rus C, Higueras PP, Hontorio L. Calculation of the energy provided by a PV generator. Comparative study: conventional methods vs. artificial neural networks. Energy 2011;36:375–84.
[86] Osterwald CR. Translation of device performance measurements to reference conditions. Solar Cells 1986;18:269–79.
[87] Green MA. Solar cells: operating principles, technology and system application. New Jersey: Prentice-Hall; 1982.
[88] Araujo G, Sánchez E, Marti M. Determination of the two-exponential solar cell equation parameters from empirical data. Solar Cells 1982;5:377–86.
[89] Kelly NA, Gibson TL. Improved photovoltaic energy output for cloudy conditions with a solar tracking system. Solar Energy 2009;83:2092–102.
[90] Tomson T. Discrete two-positional tracking of solar collectors. Renewable Energy 2008;33:400–5.
[91] Kacira M, Simsek M, Babur Y, Demirkol S. Determining optimum tilt angles and orientations of photovoltaic panels in Sanliurfa, Turkey. Renewable Energy 2004;29:1265–75.
[92] Tina GM, Gagliano. Probabilistic modelling of hybrid solar/wind power system with solar tracking system. Renewable Energy 2011;36:1719–27.